

Short-range order in two-dimensional binary alloys

L. Ottaviano,^{1,*} B. Ressel,^{2,3} C. Di Teodoro,¹ G. Profeta,¹ S. Santucci,¹ V. Cháb,³ and K. C. Prince²
¹*Istituto Nazionale di Fisica della Materia (INFM) and Dipartimento di Fisica, Università degli Studi dell'Aquila, I-67010 Coppito (L'Aquila), Italy*

²*Sincrotrone Trieste, Strada Statale 14, Km 163.5 34012 Basovizza- Trieste, Italy*

³*Institute of Physics of the Academy of Science of the Czech Republic, Cukrovarnická 10, 16253 Prague 6, Czech Republic*
 (Received 3 April 2002; revised manuscript received 2 August 2002; published 9 January 2003)

Using variable-temperature scanning tunneling microscopy, the degree of short-range order of purely two-dimensional (2D) binary alloys on triangular lattices [$\text{Sn}_{(1-x)}-\text{Si}_x$, $\text{Pb}_{(1-x)}-\text{Si}_x$, and $\text{Pb}_{(1-x)}-\text{Ge}_x$, all showing the $\sqrt{3}\times\sqrt{3}$ $R30^\circ$ reconstruction onto Si(111) or Ge(111)] has been determined quantitatively via a statistical analysis of the atomic positions. The experimental data, also in comparison with Monte Carlo simulations, generally indicate that an effective nearest-neighbor repulsion between substitutional Si (Ge) adatoms explains with good accuracy the short-range-order features observed. This finding implies the occurrence of an ordered phase of the alloys for $x=0.33$ and, in the case of a 1:1 ratio of Sn(Pb) and Si(Ge) adatoms on the surface ($x=0.5$), demonstrates that the investigated alloys are very good practical realizations of a frustrated antiferromagnetic 2D Ising system on a triangular lattice. The implications of the observed short-range order for the electronic properties of these alloys (as a function of x) are discussed.

DOI: 10.1103/PhysRevB.67.045401

PACS number(s): 68.37.Ef, 61.66.Dk, 61.43.Bn, 68.35.Rh

I. INTRODUCTION

Two-dimensional (2D) alloys of 1/3-ML group-IV metals (Pb,Sn) and semiconductors (Si,Ge) adsorbed on Ge(111) or Si(111) surfaces are attracting considerable renewed interest due to their intriguing structural and electronic properties.^{1,2} Many other systems show both bulk and surface alloying (see Ref. 3 and references therein), whereas these binary systems are truly two dimensional, due to the negligible solubility of Sn and Pb in the substrate Si and Ge.⁴ These 2D alloys, denoted $A_{(1-x)}-B_x$ ($A = \text{Sn}$ or Pb and $B = \text{Si}$ or Ge), show at room temperature (RT) a low-energy electron diffraction (LEED) pattern of $\sqrt{3}\times\sqrt{3}$ $R30^\circ$ symmetry (hereafter $\sqrt{3}$ for brevity) generally in a wide range of the concentration x , with the adatoms located in the T_4 adsorption site.⁵ In the case of the Sn/Ge system the upper value of x is limited to 0.04,^{6,7} while for $\text{Sn}_{(1-x)}-\text{Si}_x/\text{Si}(111)$, $\text{Pb}_{(1-x)}-\text{Si}_x/\text{Si}(111)$, and $\text{Pb}_{(1-x)}-\text{Ge}_x/\text{Ge}(111)$, the A and B species can be mixed with x varying in the range 0.0–0.5.^{8–12} The two limiting cases ($x=0$) and ($x=0.5$) are traditionally referred to as α and γ phases respectively, the latter also being called the *mosaic* phase. This distinction is rather semantic, as x can be almost continuously varied in this range.^{2,6,11,13}

There are many open issues for these 2D alloys. Most of the defect-free α surfaces [Pb/Ge, Ref. 14 Sn/Ge, Ref. 15 and Pb/Si Ref. 16] undergo an intrinsic structural phase transition to a reduced 3×3 symmetry at low temperature. Nonetheless, for Sn/Ge it has been clearly demonstrated that substitutional Ge adatoms at $x=0.04$ undergo a disorder-order phase transition with the same symmetry lowering.¹⁷ This interplay of two types of phase transitions with the same type of symmetry lowering might reasonably occur also for the Pb/Si and Pb/Ge cases. Despite clear indications of a 3×3 ground-state symmetry,^{2,18} α -Sn/Si does not show this structural transition at low temperature,^{18,19} so that in-

vestigation of the defect-induced structural phase transition is especially worthwhile for this system. For the mosaic phase ($x=0.5$), filled-state scanning tunneling microscopy (STM) images show a characteristic short-range order (SRO) with alternating kinked lines of the two adatom species: it seems that a local $2\sqrt{3}\times\sqrt{3}$ unit cell can be discerned. The local order and simple electron counting arguments (two electrons per unit cell) lead one to expect that the surface is semiconducting.¹² Also, early researchers have mentioned the mosaic surface as a possible practical realization of a 2D antiferromagnetic Ising system on a triangular lattice,^{10,12} but have not developed this idea.

For binary bulk systems (with A and B atoms), which possess short-range but no long-range order, the determination of the A - A , B - B , and A - B pair distribution functions (PDF's) is of primary interest. Given a reference A (or B) adatom site the P_{AA} (or P_{BB} or P_{AB}) PDF gives the shell occupancy probability of like (P_{AA}, P_{BB}) or unlike (P_{AB}) atoms as a function of the shell coordination number (SCN). This information is directly accessible in 2D systems with STM. Via a statistical analysis of the STM images, the PDF can be determined for the A - and B -type adatoms of the binary solution. To our knowledge, this type of quantitative analysis has been attempted only for the surfaces of metallic 3D binary systems (see Ref. 3 and references therein). In combination with direct experimental investigation, Monte Carlo (MC) stochastic computer simulations²⁰ represent a standard powerful nonanalytical approach to study binary alloys and the ordering phenomena occurring at their surfaces.²¹

In this paper we present a quantitative determination of the Si-Si (Ge-Ge) PDF (determined from STM images) for the Sn-Si, Pb-Si, and Pb-Ge 2D alloys as a function of x and temperature as summarized in Table I. The experimental PDF's have been compared with those obtained from a very simplified Monte Carlo simulation of a lattice gas model on a triangular lattice assuming only nearest-neighbor (NN) in-

TABLE I. Summary table of the observed alloys as a function of Si (Ge) surface concentration and temperature.

Alloy	Si(Ge)%	RT	LT
Sn-Si	14	<i>x</i>	-
Sn-Si	30	<i>x</i>	100 K
Sn-Si	49	<i>x</i>	30 K
Pb-Si	50	<i>x</i>	-
Pb-Ge	40	<i>x</i>	-

teractions between substitutional adatoms. Section II of this paper briefly describes the experimental setups used; details are given of the calculation of the PDF's and of the Monte Carlo simulations. In Sec. III the Si-Si (Ge-Ge) experimental PDF's [hereafter $P_{\text{Si}}(s)$ and $P_{\text{Ge}}(s)$] are presented and compared to those of reference ordered phases at corresponding x values. In Sec. IV the results of the Monte Carlo simulations are given and discussed in comparison with the experimental results. Finally in Sec. V the conclusions are given.

II. DETAILS OF THE EXPERIMENT, CALCULATION OF THE PDF'S, AND MC SIMULATIONS

Details of the experimental systems used and of the sample preparation procedures are given elsewhere.^{2,22} In the case of Sn/Si, the STM coverage corresponding to 1/3 ML was calibrated according to the work of Uhrberg *et al.*¹⁸ Starting from the nearly perfect $\sqrt{3}$ surface we finely tuned the surface density of substitutional Si atoms by further annealing the samples at various temperatures up to 870 °C.² The Pb/Si(111) mosaic phase was obtained after deposition of 0.6 ML lead and annealing for 3 min at 500 °C. For the experimental determination of the PDF's, we used filled-state STM images. These images always exhibit a strong contrast of the two adatom species when tunneling into filled states [about 1.5–2.0 V (Refs. 8–12 and 22)] Sn (Si) adatoms appear bright (dark) in these images. The assignment of substitutional (semiconductor) adatoms to the dark sites in the filled-state images of these alloys (and vice versa) has been established by quantitative comparison of STM with core-level spectroscopy data.² In our experimental determination of the function $P_{\text{Si}}(s)[P_{\text{Ge}}(s)]$ for the Si [Ge] substitutional adatoms we considered high-quality large-area ($30 \times 30 \text{ nm}^2$) filled-state STM images (as in Fig. 1). The estimated concentration of vacancies (which appear dark in both empty- and filled-state images) was very low (1%–2%). Their low concentration does not affect the equilibrium properties of the alloys considered, but may play an important role in the diffusion of the two adatom species.²³ The scan size has been chosen as a good compromise between the competing needs of atomic resolution and a sufficiently large number of adatoms to be analyzed. In a triangular reference system determined by the unit lattice vectors of the surface, the position of each adatom can be stored as a pair of integer numbers (j, k) so that its vector position is $\mathbf{R} = j\mathbf{a} + k\mathbf{b}$. For statistical analysis we considered the adatoms inside a $J \times K$ supercell ($J \approx K \approx 30$) that is a rhomboidal portion of the overall scanned area. Accordingly, the overall number of

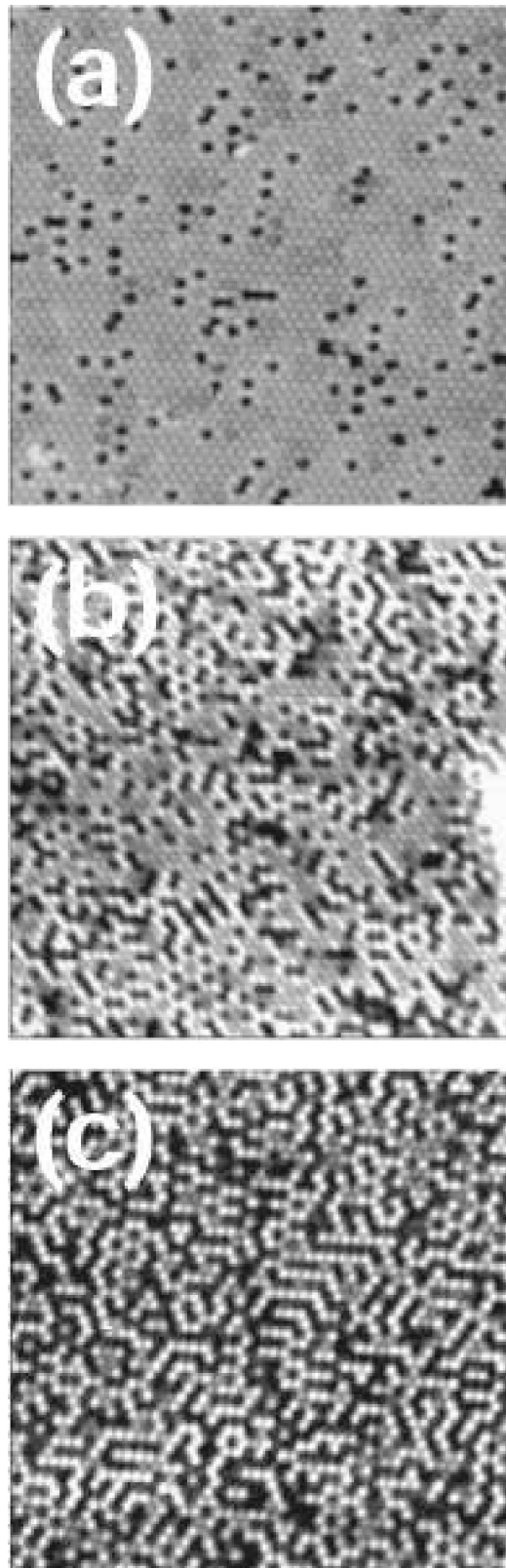


FIG. 1. RT filled-state (-1.5 V , 0.5 nA , $30 \times 30 \text{ nm}^2$) STM images of the $\text{Sn}_{(1-x)}\text{Si}_x/\text{Si}(111)$ 2D alloy for (a) $x=0.14$, (b) $x=0.30$, and (c) $x=0.49$ (mosaic phase). Sn adatoms are bright; Si are dark.

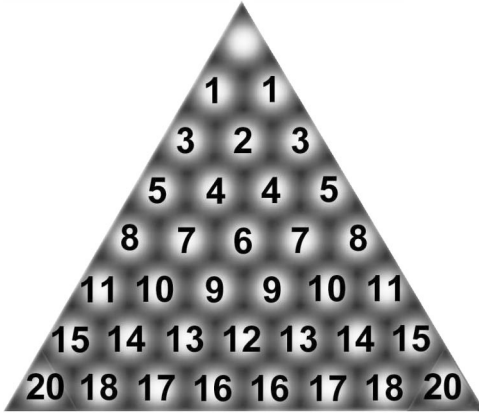


FIG. 2. Triangular portion of a diagram of a surface with atoms in a triangular arrangement, reproducing the surface symmetry of the considered α surfaces. The atoms are labeled with the corresponding number of the coordination shell with respect to the top-most atom.

Si adatom positions stored is sufficiently large (varying from a minimum of about 130 [14% Si] to a maximum of about 450 [50% Si]) to measure the experimental $P_{\text{Si}}(s)$ [or $P_{\text{Ge}}(s)$] functions with good accuracy up to the 20th coordination shell. This shell coordination number corresponds to a distance of 46.5 Å (48.9 Å for the Ge substrate) from the reference atom. We verified that the choice of 20 as maximum SCN is in general of the order of 3–4 times the highest SCN of the atoms significantly correlated with the reference atom. It is worth noting that any type of significant order present in the $P_{\text{Si(Ge)}}(s)$ functions up to this maximum SCN value should be evident in a LEED pattern (typical electron coherence length of the order of 100 Å). This defines our spatial range of investigation. Figure 2 shows a diagram of the position of each coordination shell, up to the 20th. Further details of the determination (and corresponding error calculation) of the PDF's from STM images (or MC simulations) are given in the Appendix.

The MC simulations assume an effective model interaction, and then the simulation proceeds according to the usual standard Metropolis criterion.²⁰ In our case an effective NN pairwise repulsive energy between substitutional adatoms B on a substrate A is used:

$$U(r=0) = \infty,$$

$$U(r=r_1) = \varepsilon,$$

$$U(r>r_1) = 0,$$

where r_1 is the nearest-neighbor distance in the 2D lattice. According to this model the Hamiltonian of this 2D system is

$$H = \frac{1}{2} \varepsilon \sum_{i=1}^N \sum_{j=1}^6 x_i y_j, \quad (1)$$

where x_i , y_j are equal to 1 if the site i or j of the lattice is occupied by an atom of B and 0 otherwise.

This is a lattice gas model on a triangular lattice (six neighbors).

For the dynamics of the simulations, at each step the chemical identity of two (chemically different) random sites is switched and the new configuration is accepted according to the Metropolis criterion.²⁰ This type of dynamics for the simulation has already been used to investigate the surface short-range chemical ordering in a binary alloy.²⁴

For a configuration of N atoms on this lattice, the total energy of the system will be ε times the number of nearest-neighbor pairs of adatoms. The MC simulations were done considering N atoms in a $J \times K$ supercell (with the repeated supercell geometry) with N , J , and K equal to the corresponding values determined experimentally at the various Si (Ge) adatom densities considered. We started from a random distribution of the N particles in the $J \times K$ lattice sites. Equilibrium was judged by monitoring the slope (calculated at each MC step over the previous 20 MC steps) of the curve of the average nearest-neighbor coordination number of like atoms as a function of time (MC step). Equilibrium was considered to be reached once this slope oscillated between zero and $k_B T / (20\varepsilon)$. The only adjustable parameter in the simulations was the reduced energy $\varepsilon^* = \varepsilon / k_B T$ (vice versa the reduced temperature is $T^* = 1/\varepsilon^*$). Once equilibrium was reached (typically after 10^5 steps corresponding to an average of 10^3 steps per simulated particle) the equilibrium configuration (the ensemble of coordinates of the particles) was stored and the corresponding P_{Si} and P_{Ge} functions were calculated as for the experimental data.

III. THE EXPERIMENTAL PDF'S

We postulate that the PDF is characteristic of the SRO and that the first few shells are similar to the long-range-ordered phases at corresponding values of x . To check this we have analyzed (see Fig. 3) the ordered phases with the lowest-size unit cells that can be generated for $x=0.33$ and $x=0.5$ (corresponding to the experimental x values; see Table I). For $x=0.33$ the lowest-size unit cell is 3×3 with two bright and one dark atom per unit cell, usually referred to as 3×3 hexagonal in the literature²⁵ [see right portion of Fig. 3(e)]. The corresponding PDF of dark atoms is given in Fig. 4 (open triangles). For $x=0.5$ we have generated all of the possible unit cells up to a cell size of $3\sqrt{3} \times 2\sqrt{3}$ and considered all possible arrangements within the unit cell that give $x=0.5$. As well we have considered the mixture of 3×3 structures [Fig. 3(e)], which also gives the correct stoichiometry, and some larger unit cells. The correspondingly calculated PDF's are shown in Fig. 4.

We emphasize that, these PDF's are calculated from ordered phases, and thus they are reported with exact values (no error bars). The various PDF's for $x=0.5$ are distinguishable. For example, the line phase [Fig. 3(a)] shows an increased occupation probability in the third shell while this occurs in the fourth shell for the zigzag phase [Fig. 3(b)]. These phases are both different from those of Fig. 3 [panels (c), (d), and (e)] that are qualitatively similar one another. We use these reference PDF's to assign the type of SRO observed experimentally.

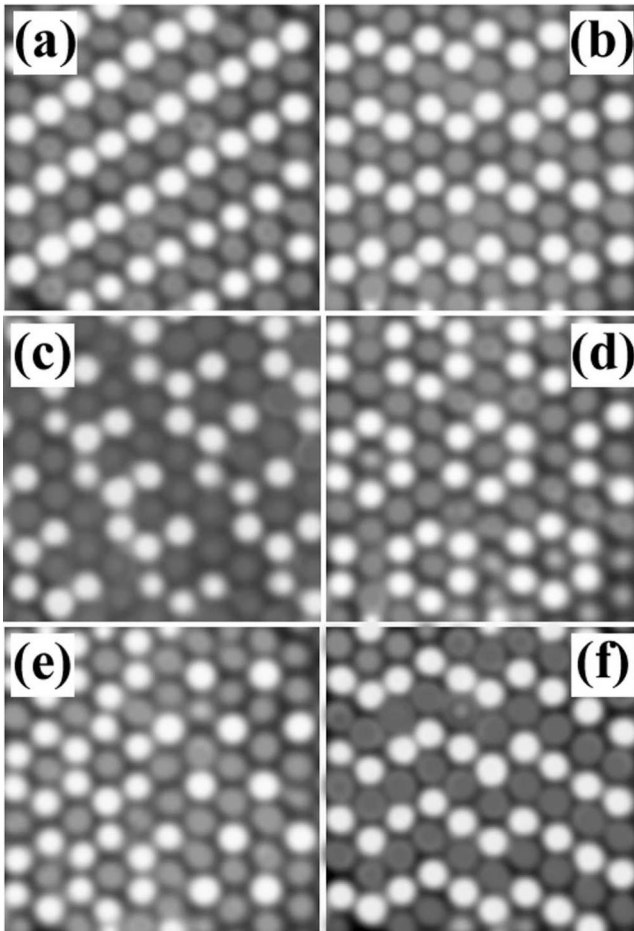


FIG. 3. Ball model images of various ground-state configurations for the (frustrated) antiferromagnetic Ising system on a triangular lattice. (a) Line phase ($2\sqrt{3} \times \sqrt{3}$, one dark and one bright atom per unit cell), (b) zigzag phase ($2\sqrt{3} \times 3$, two dark and two bright atoms per unit cell), (c) comb phase ($3\sqrt{3} \times 3$, three dark and three bright atoms per unit cell), (d) pinwheel phase (6×6 , six dark and six bright atoms per unit cell), (e) surface partitioned with bright atoms arranged into a 3×3 ($x=1/3$) (left portion) and 3×3 ($x=2/3$) (right portion), and (f) kinked line phase (no long-range order).

Figure 5 shows the room-temperature $P_{Si}(s)$ functions of the Sn-Si surface as a function of the Si adatom density (14%, 30%, and 49%). First, in all the experimental $P_{Si}(s)$ in Fig. 5 [as well as for $P_{Si}(s)$ and $P_{Ge}(s)$ in Fig. 6] the first coordination shell always shows the most significant deviation from the oscillation range expected from a random distribution (gray bands in Fig. 5 and Fig. 6). This happens also at rather low Si densities at RT [14% in Fig. 5(a) and 10% not presented for brevity]. The deviation from the random oscillation range of $P_{Si}(1)$ is not the only significant information in Fig. 5(a). This $P_{Si}(s)$ shows that the arrangement of Si atoms from the second shell onward is in agreement with a random distribution. Thus, there is a Si-Si interaction practically limited to the first shell, and, at least at RT, the interaction energy at larger distances is negligible in comparison with the thermal energy. This observation justifies the model interaction energy of Sec. IV. Panel (b) of Fig. 5

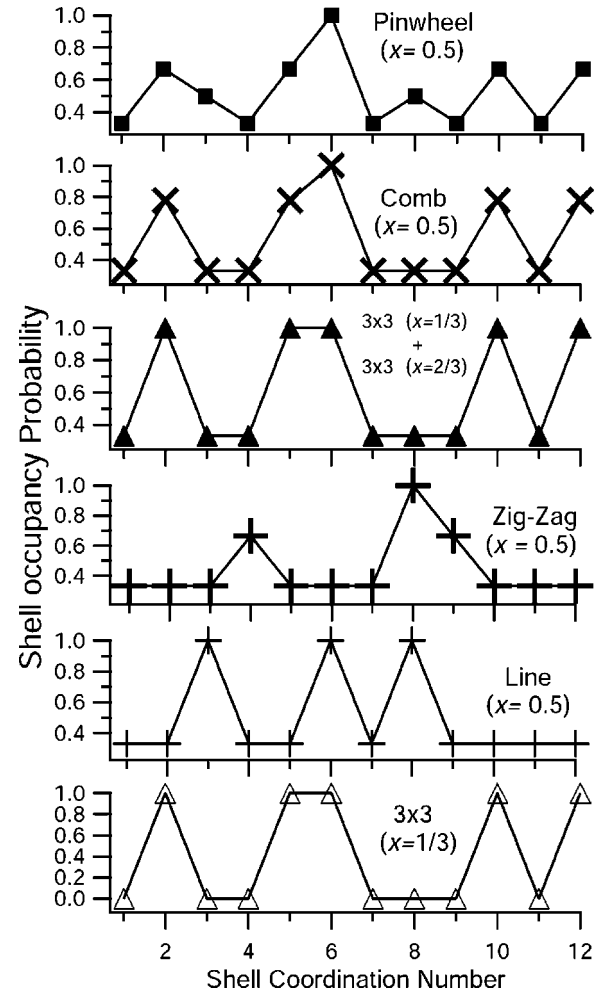


FIG. 4. Shell occupancy probability for the various ordered phases at $x=0.3$ and $x=0.5$ of Fig. 3. From bottom to top: (open triangles, Δ), 3×3 phase at $x=0.33$ coverage, (+) line phase ($2\sqrt{3} \times \sqrt{3}$), (+, bold) zigzag phase ($2\sqrt{3} \times 3$), (solid triangles) weighted average of 3×3 ($x=2/3$) (weight=1) and 3×3 ($x=1/3$) (weight=2), (\times) comb phase ($3\sqrt{3} \times 3$), and (solid squares, \blacksquare) pinwheel phase (6×6).

shows the Si-Si pair correlation function for $x=0.3$: there is marked SRO. The experimental points that significantly deviate from the oscillation range of the corresponding random distribution are those of shells 1, 2, 4, 5, and 6. Shells 1 and 4 are significantly depleted, shells 2, 5, and 6 are significantly populated, and from the seventh shell onward the distribution is random. Taking account of thermal disorder, up to the sixth shell this is the same behavior of the PDF of the 1/9-ML 3×3 triangular ordered phase (Fig. 4, open triangles) of this coverage. So at $x=0.3$ there is local 3×3 triangular order of the Si adatoms and of the Sn adatoms (2/9-ML coverage).

The pair correlation function measured for the concentration value $x=0.49$ shows a different type of SRO [Fig. 5(c)], which can also be observed with similar qualitative features at higher (0.54) and lower (0.44) values of the Si adatom concentration (data not shown for brevity). The coordination shells significantly outside the oscillation range for a random

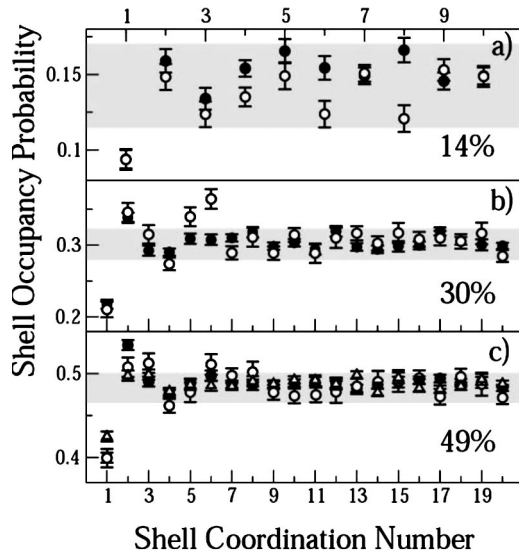


FIG. 5. RT Si-Si adatom correlation functions at various surface concentrations, 14% (a), 30% (b) and 49% (c) for the $\text{Sn}_{(1-x)}\text{Si}_x/\text{Si}(111)$ 2D alloy. Open circles (\circ) are experimental values from the statistical analysis of STM filled-state images (see Fig. 1). The shell occupancy probability is normalized to the multiplicity of each shell; i.e., numbers 4, 7, 9, 10, 13, 14, 16, 17, and 18 accommodate 12 atoms each and the others 6. Solid circles (\bullet) are the corresponding data from a MC simulation with the effective temperature tuned in order to have $P_{\text{Si}}(1) = P_{\text{MC}}(1)$. The horizontal gray band corresponds to the oscillation range of the occupancy values in the hypothesis of the Si random distribution. In panel (c) the open triangles (\triangle) correspond to a MC simulation at higher effective temperature ($T^* = 2$). In panel (a) two data points (experimental and MC) are superimposed at the first SCN.

distribution are 1, 2, 3, 4, 6, and 8. Shells 1 and 4 are significantly depleted, while shells 2, 3, 6, and 8 are significantly more populated. Comparison now is possible and instructive with the PDF's of the ordered phases at $x = 0.5$ with the smallest unit cells reported in Fig. 4. The experimental PDF does not resemble the zigzag phase. Significant occu-

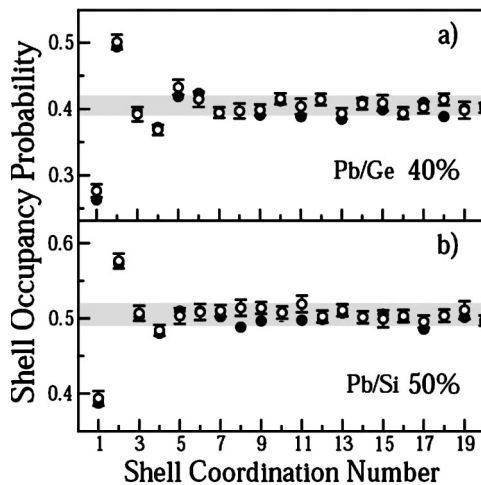


FIG. 6. Same as Fig. 5 for (a) $\text{Pb}_{0.6}\text{Ge}_{0.4}/\text{Ge}(111)$ and (b) $\text{Pb}_{0.5}\text{Si}_{0.5}/\text{Si}(111)$ at RT.

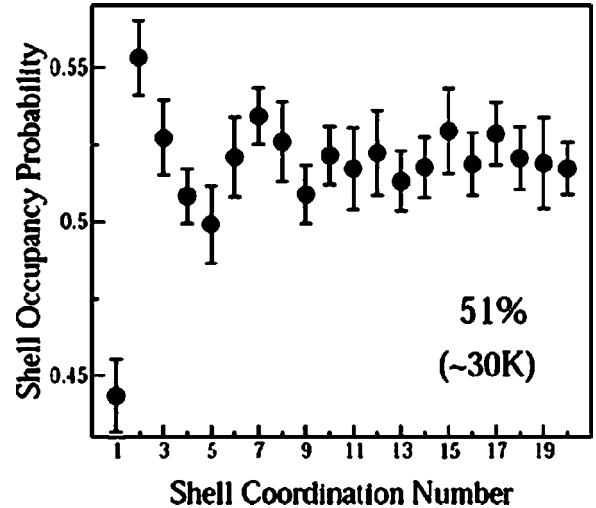


FIG. 7. Si-Si PDF calculated from a filled-state STM image of the $\text{Sn}/\text{Si}(111)$ mosaic phase (49% Si) at 30 K .

pation of shell 2 is observed for the PDF of the weighted 3×3 (or $3\sqrt{3} \times 3$ comb or 6×6 pinwheel) phase, but significant occupation of shells 3, 6, and 8, no significant occupation of shell 5, and significant depletion of shell 4 are unique features of the $2\sqrt{3} \times \sqrt{3}$ (line) type short-range order.

This is not observed for the mosaic Pb/Si and Pb/Ge phases. The $P_{\text{Si}}(s)$ and $P_{\text{Ge}}(s)$ functions of Fig. 6 have been calculated from the statistical analysis of $\gamma\text{-Pb}/\text{Si}$ (STM images reported elsewhere²⁶) and of published data of $\gamma\text{-Pb}/\text{Ge}$ [namely, Fig. 3(a) in Ref. 12]. These two surfaces show a significant difference of the type of SRO observed for the Sn/Si mosaic phase and $P_{\text{Si}(\text{Ge})}(3) < P_{\text{Si}(\text{Ge})}(2)$. Surprisingly there is no sign in these $P_{\text{Si}}(s)$ and $P_{\text{Ge}}(s)$ functions of the line type SRO often claimed as a qualitative feature “visible at first glance” in these systems, as there is no resemblance at a qualitative level of the measured PDF's with the ordered $2\sqrt{3} \times \sqrt{3}$ phase. Indeed, it is easy to recognize also for these surfaces at this high concentration of substrate adatoms that the type of SRO is still consistent with the PDF of the weighted 3×3 (or $3\sqrt{3} \times 3$ or 6×6) phase. In particular, the 3×3 type SRO in $\gamma\text{-Pb}/\text{Si}$ is substantially limited to the NN and next NN (NNN) atoms, while in the case of $\gamma\text{-Pb}/\text{Ge}$ this type of SRO extends a little further up to the fifth shell.

The same type of SRO observed for $\gamma\text{-Pb}/\text{Si}$ and $\gamma\text{-Pb}/\text{Ge}$ at RT is observed for $\gamma\text{-Sn}/\text{Si}$ at reduced temperature (30 K) as shown in Fig. 7 where, as for the other γ phases considered at RT, one has $P_{\text{Si}}(3) < P_{\text{Si}}(2)$. This is an important finding because it implies that Sn-Si rearrangement must occur when the temperature is reduced. There is no direct experimental evidence to indicate the mechanism of such a rearrangement, but it is plausible that it takes place through vacancy-assisted hopping of the adatoms.²³ In summary, as far as the SRO features are concerned, $\gamma\text{-Pb}/\text{Si}$ and $\gamma\text{-Pb}/\text{Ge}$ are like one another at RT and similar to LT $\gamma\text{-Sn}/\text{Si}$.

IV. MONTE CARLO SIMULATIONS AND DISCUSSION

The choice of Eq. (1) for the effective Hamiltonian of the system is a simplification which we justify as follows. First,

the experimental PDF's clearly suggest an effective repulsion between substitutional adatoms. Furthermore, Ortega *et al.*²⁷ have demonstrated that for Sn/Ge, adsorption of Ge adatoms on neighboring T_4 sites is not energetically favored and the second NN site is preferred. The presence of a substitutional adatom produces a very localized lattice distortion that moves the Sn NN adatoms upward and effectively repels other substitutional adatoms. The energy gain is calculated to be 160 meV,²⁷ and due to the very localized structural distortion, no further gain in energy is obtained if the substitutional adatom is placed further away. Sn and Pb show the $\sqrt{3}$ reconstruction both on Si(111) and Ge(111) and this repulsive effective interaction does not appear to exist for these adatoms. Thus while in MC simulations of these alloys one should in principle account for the Sn-Sn (Pb-Pb), Sn-Si, Pb-Ge, and Si-Si (Ge-Ge) interactions, the proposed model interaction can be expected to work by only considering the interactions of the substitutional adatoms. For the same reasons we have calculated and reported only the Si-Si (Ge-Ge) experimental PDF's in Figs. 5, 6, and 7. The results presented in the following section demonstrate the ability of this effective interaction to reproduce the SRO features observed experimentally. Thus, our choice for the model interaction 1 is substantially justified *a posteriori*.

The calculated PDF's from the MC simulations for the various substitutional adatom densities determined experimentally are reported (solid circles) in Figs. 5 and 6. Since the effective NN interaction energy ε is unknown *a priori*, the reduced energy ε^* for each simulation has been adjusted so that $P_{\text{Si(Ge)}}(1) = P_{\text{MC}}(1)$. As the experimental PDF's have been determined from STM images at RT ($k_B T \approx 26$ meV), this gives an absolute estimate of ε . This value is 32.0 ± 0.5 meV both for γ -Pb/Si and γ -Pb/Ge, while for γ -Sn/Si it is 10 ± 2 meV (independent of the concentration). The stronger effective interaction strength measured in the case of the alloys with Pb adatoms with respect to Sn can be traced back to the different atomic radii of these adatoms (1.80 Å and 1.45 Å for Pb and Sn, respectively). Pb protrudes outward more than Sn from the Si(Ge)(111) substrate plane. The further outward it protrudes, the more effective is the dehybridization of the Pb dangling bond state that acquires *s* character,²⁸ and the more effective is the complete filling of this state. We conjecture that this dehybridization can be even more significant for Pb when there is a Si (or Ge) neighbor at the surface.

In the case of γ -Pb/Si (Ge) (Fig. 6) the results of the MC simulated PDF's are in excellent agreement with the corresponding experimental functions. The agreement between the model MC simulations and the experimental PDF's is a bit less satisfactory in the case of the Sn-Si binary alloy (Fig. 5). For $x=0.3$ the calculated SCN's 5 and 6 are not well reproduced and the real alloy has more extended 3×3 SRO than the simulated alloy at the corresponding Si adatom concentration and temperature. For the mosaic phase [Fig. 5(c)] in contrast with the experimental results, the MC simulation yields $P_{\text{MC}}(3) < P_{\text{MC}}(2)$ (as in Fig. 6). Nonetheless, if the constraint $P_{\text{Si}}(1) = P_{\text{MC}}(1)$ is relaxed and the MC simulation is performed at higher temperature, the experimentally observed features of the PDF of the γ -Sn/Si can be quite well

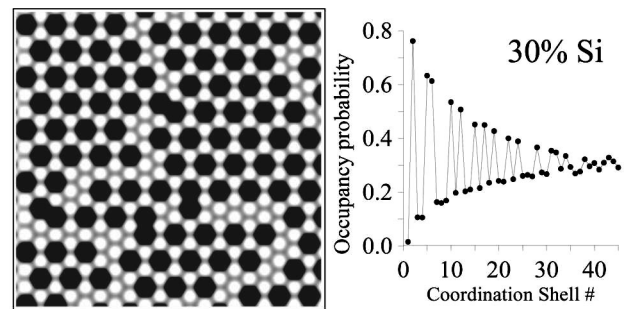


FIG. 8. Left: simulation of the STM images of a 2D solid solution on a triangular lattice for 30% surface concentration of dark (substitutional) atoms at $T^* = 0.1$. Right: corresponding PDF.

qualitatively reproduced [triangles in Fig. 5(c)]. In particular, the SRO feature $P_{\text{Si}}(3) > P_{\text{Si}}(2)$ observed experimentally can be qualitatively reproduced. Both MC and the estimate of the effective interaction energy for γ -Sn/Si indicate that this 2D alloy at RT can be considered as a system like the similar γ -Pb/Si(Ge) ones but at higher temperature. As a general rule, the MC simulations based on only the Si-Si (Ge-Ge) NN repulsive interaction can describe with good accuracy the structural features of this class of binary alloys. Due to the crude approximation of the model interaction used [with no Sn-Sn (or Pb-Pb) adatom interaction and with the Si-Si (Ge-Ge) effective interaction truncated at the first neighbors], what is surprising is the excellent agreement of simulation and experiment in Fig. 6, and not their slight discrepancies in Fig. 5.

From the preceding, when $x=0.33$ an ordered 3×3 phase (with two Sn and one Si per unit cell) should be observed at reduced temperature for the Sn/Si interface (there is already 3×3 SRO at $x=0.3$ at RT, and the general validity of the NN model interaction implies such an ordered ground state at $x=0.33$). Moreover, we have demonstrated that Si adatoms rearrange with temperature, as in the MC simulations due to this effective interaction. Figure 8 shows that for $x=0.30$ and $T=20$ K, one obtains a MC-simulated STM image where the black and white adatoms are ordered in 3×3 unit cells over domains of the order of five to six cells in diameter. In a real experiment on the Sn/Si surface this would correspond to domains of the order of $100 \times 100 \text{ \AA}^2$, sufficiently large to produce sharp 3×3 spots in a LEED pattern. Indeed, Fig. 9 provides some experimental support for this prediction. The figure presents the 100 K LEED pattern of a $1/3$ -ML $\text{Sn}_{0.7}\text{Si}_{0.3}/\text{Si}(111)$ surface. There is a clear 3×3 modulation of the background of the $\sqrt{3}$ pattern. A spot profile analysis of the nascent 3×3 spots (inset in Fig. 9) indicates that the size of the 3×3 islands is about 20–30 Å. This type of 3×3 background at reduced temperature is neither observed for lower ($x < 0.25$) nor for higher ($x > 0.35$) values of the Si adatom concentration, so it is related to Si-Si ordering. Our results provide a simple explanation for the lack of observations of this phase transition at 100 K. The interaction energy we find for Sn/Si is 10 meV, a factor of about 3 lower than for Pb/Si and Pb/Ge. The critical temperatures for the 3×3 phase transition in these cases are 60 K and 210 K, so we expect the critical temperature in the

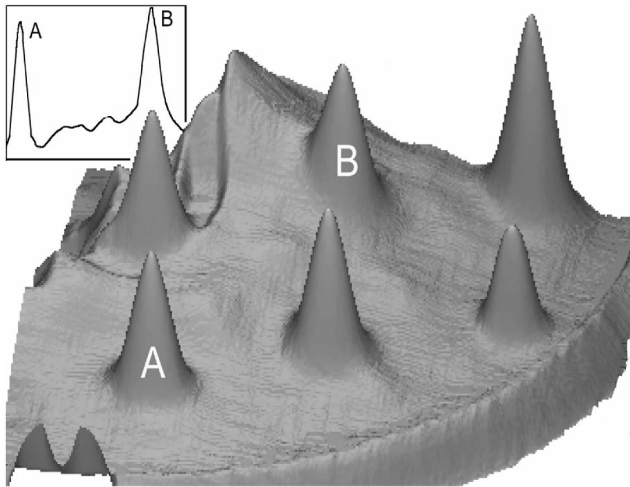


FIG. 9. 3D representation (and intensity profile drawn between the 1×1 spots labeled *A* and *B*) of the LEED pattern (46 eV beam energy) of the $1/3$ -ML $\text{Sn}_{0.70}\text{Si}_{0.30}/\text{Si}(111)\sqrt{3} \times \sqrt{3}$ surface at 100 K. 3×3 spots are visible above the background.

Sn/Si case to be roughly a factor of 3 lower—that is, 20 to 70 K. However, at these low temperatures, diffusion is likely to be very slow, and it is likely that equilibrium cannot be achieved in reasonable experimental times.

In the case of $x=0.5$, by using a little algebra it can be demonstrated that, apart from constant terms, the effective Hamiltonian H of Eq. (1) coincides with the antiferromagnetic Ising model on a triangular lattice.²⁹ This system is highly frustrated because a single atom would ideally minimize its energy by being surrounded by six atoms of opposite type. However, the surrounding atoms cannot in turn minimize their energy, as they each necessarily have at least two like neighbors. This is in contrast to Ising systems on square and rectangular lattices, where minimization can be achieved. In the ground state of this model, the average coordination is four atoms of opposite and two atoms of the same spin (chemical identity in this case). There is an infinite number of ordered and disordered ground states for this system. The ordered phase shown in Figs. 3(a), 3(b), 3(c), and 3(d) all correspond to possible ground states of the Ising system (they all have two out of six like NN; see Fig. 4). Evidently there is an infinite number of other ordered phases with larger unit cells and we show only those with smaller unit cells (for instance, in a $3\sqrt{3} \times 3$ or 6×6 unit cell a different choice of the position of the bright and dark atoms produces other ordered phases). Note that kinks in the chains of Fig. 3(a) do not raise the energy as all atoms retain the same coordination number [see Fig. 3(f)]. Thus, any kinked structure is also in the ground state. In an infinite system, the number of permutations for arranging the kinks is also unlimited and so the system is infinitely degenerate. Finally, a 3×3 ordered ground state may also exist for the Ising model as visualized in Fig. 3(e). The left-hand portion of the surface is 3×3 ($x=1/3$, $2/3$ bright and $1/3$ dark atoms), and the right-hand one is 3×3 ($x=2/3$, $1/3$ bright and $2/3$ dark). The overall bright to dark ratio is 1:1, the average coordination number of like atoms is 2, and it can be easily shown

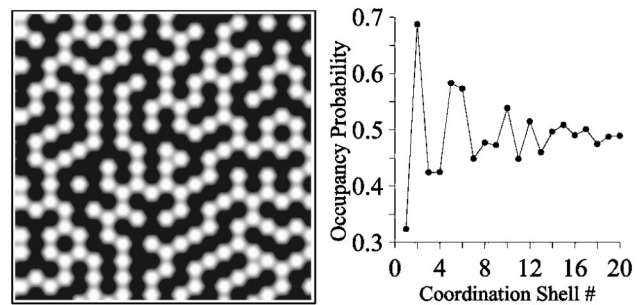


FIG. 10. Left: simulated STM image from a MC simulation of a 2D solid solution on a triangular lattice for 50% surface concentration of dark atoms (antiferromagnetic Ising limit) at $T^*=0.01$. Right: corresponding PDF.

that the domain wall does not cost additional energy, so this is also a ground state. Inspection of all these phases shows that while the nearest-neighbor coordination number is well defined, the coordination number in the second and higher shells varies according to the particular model (see Fig. 4). The real coordination number for SCNs higher than 1 can only be estimated from a statistical average of all possible configurations. Average functions calculated from MC calculations give an idea of the occupation probability of higher shells.

Thus, on the one hand, our results, indicating that these alloys with $x=0.5$ are very good practical realizations of an antiferromagnetic Ising system on a 2D triangular lattice, quantitatively confirm previous speculations made in Refs. 10 and 12. On the other hand, we have illustrated that the line phase of Fig. 3(a) is just one of an infinite number of ground states for an Ising system and that investigation of the occupancy probabilities of SCN higher than 2 in the PDF of like atoms provides insight into the SRO.

Figure 10 (left) shows the appearance of the triangular Ising system after a MC simulation at very low reduced temperature ($T^*=0.01$) based on the interaction energy found in this work. Figure 10 (right) reports the corresponding PDF (for the dark atoms). The occupancy probability of the first shell is indeed close to 0.33, so this is a typical Ising ground state. There is significantly increased occupancy of shells 2, 5, 6, 10, and 12, while shells 3, 4, 7, 8, 9, and 11 are significantly depleted. These SRO features are in disagreement with those of the line and zigzag phases represented in Fig. 3 [panels (a) and (b)], whose PDF's are reported in Fig. 4. The pinwheel phase [see Fig. 3(d)] predicts 0.5 occupancy probability of the third shell (topmost graph in Fig. 4), while it is observed to be significantly depleted in Fig. 8, so it should be also ruled out. Instead, there is good qualitative agreement with the PDF's typical of the comb $3\sqrt{3} \times 3$ phase and the weighted average of the 3×3 phases [see Figs. 3(c) and 3(e) and Fig. 4, second and third graphs from the top]. We therefore conclude that there is significant short-range order with threefold periodicity. Since the PDF does not give angular information, we cannot say much about what a unit cell might be, but the smallest appears to be (3×3) .

The results obtained by the MC simulations and the analysis of the STM images provide insight into the electronic structure of the mosaic phase. There is experimental

evidence that the γ phase of these systems is semiconducting, from angle-resolved ultraviolet photoemission spectroscopy³⁰ (ARUPS) and STM-STS³¹ experiments for γ -Pb/Si and from STM-STS experiments¹ for γ -Sn/Si. In the case of the Pb/Ge mosaic phase, Carpinelli *et al.*¹² have clearly demonstrated the opening of a 0.37-eV gap. This is consistent with electron counting arguments if the single-particle band structure theory is assumed to be valid and if a $2\sqrt{3} \times \sqrt{3}$ unit cell is adopted as a reference system (with one Si and one Sn in the basis). The present work has demonstrated that this type of SRO can certainly be excluded for γ -Pb/Si(Ge) at RT and γ -Sn/Si at low temperature, so the semiconducting nature of these surfaces requires a more sophisticated explanation. Apart from γ -Sn/Si at RT, we have demonstrated that the SRO features of the mosaic phases are consistent with those of a weighted average of 3×3 ($x = 1/3$) and 3×3 ($x = 2/3$) phases (or phases with larger unit cell like the $3\sqrt{3} \times 3$ and the 6×6). The $2\sqrt{3} \times \sqrt{3}$ approximation is too simple, and band broadening due to Si-Si and Sn-Sn interactions in a larger unit cell could modify substantially the electronic properties of the surface. For example, there should be, respectively, 6 and 12 surface bands if the more realistic $3\sqrt{3} \times 3$ and 6×6 phases are considered. Moreover, we have demonstrated that partitioning of the mosaic surface into 3×3 islands with 33% and 66% coverage, respectively, also produces a possible ground state of the mosaic surfaces, and this is consistent with the observed SRO features. Thus, a 1:1 ratio of the metal and semiconductor surface adatoms in the mosaic surfaces is not sufficient to exclude *a priori* their metallic nature. Evidently there is still insufficient experimental spectroscopic information and a thorough reinvestigation of the electronic structure of these alloys using STS with atomic resolution and first-principles calculations would be worthwhile. With regard to the electronic properties, we will present a fuller discussion elsewhere.³²

V. CONCLUSION

The SRO features of purely two-dimensional binary alloys (Sn-Si, Pb-Si, and Pb-Ge) have been determined quantitatively (up to the 20th SCN) by means of statistical analysis of filled-state STM images. A threefold translational symmetry governs the mutual arrangement of the substitutional adatoms (Si and Ge) regardless of their density. MC simulations show that the SRO features observed in these alloys can be reproduced if a simple effective NN repulsion is assumed only between substitutional adatoms. The strength of this effective repulsion is 30 meV for the Pb-Si and Pb-Ge alloys and 10 meV for Sn-Si. At $x = 0.33$ a (3×3) order-disorder transition is predicted, and experimental indications are given of its possible onset. Full ordering at low temperature appears to be kinetically limited by the diffusion process. In the limit of 1:1 ratio of the two adatom species in the case of γ -Pb/Si(Ge) these systems are a practical realization of a 2D antiferromagnetic Ising system on a triangular lattice.

In general, our results are in agreement with the theoretical and experimental view that Sn/Si is more complicated

than the other surfaces. The very localized nature of the effective NN Si-Si (Ge-Ge) interaction with negligible contributions from second NN remains to be explained hopefully with more fundamental theoretical work.

ACKNOWLEDGMENTS

C.D.T. acknowledges financial support from the SOCRATES Project of the European Union. Valuable experimental support from Dr. Jiri Slezák is also acknowledged. Financial support of the Czech Grant Agency is acknowledged (Grant No. 202/98/K002).

APPENDIX

In general, for N adatoms of B type (B either Si or Ge) in the supercell, one calculates all the $N(N-1)/2$ independent values of the B - B distances. If (ξ_1, η_1) and (ξ_2, η_2) are the coordinates of two adatoms in the triangular reference system of the supercell, then it can be easily shown that their distance d satisfies the following relation:

$$d^2 = \Delta \xi^2 + \Delta \eta^2 + \Delta \xi \Delta \eta,$$

where

$$\Delta \xi = \xi_1 - \xi_2$$

and

$$\Delta \eta = \eta_1 - \eta_2.$$

There is a one-to-one correspondence between the values of d^2 and the SCN s . Thus, counting the number of independent couples of adatoms that give the same value of the square distance d^2 will give the number of independent couples of adatoms that are s th neighbors of one another. Renormalizing this number by the total possible number of s neighboring lattice sites within the supercell will finally yield the probability $P_B(s)$ of the occupation of the s SCN. In our experimental determination of the $P_B(s)$ functions we did not adopt the repeated supercell geometry in the statistical analysis code, and the truncation effects due to the finite size of the supercell are accounted for in the renormalization procedure (counting of the site-dependent neighboring lattice sites of the s th shell) of the observed experimental frequencies. Since $P_B(s)$ is the estimate of the occupation probability of the s th shell, $1 - P_B(s)$ is the probability of nonoccupation. Thus, given a reference B adatom, the probability of finding an atom B in the s th shell obeys a binomial distribution probability with mean value $P_B(s)$ and variance $P_B(s)[1 - P_B(s)]\nu_s$ (ν_s being the measured experimental frequency of the s th shell). Accordingly the error in the estimate of $P_B(s)$ will be

$$\sigma(s) = \{P_B(s)[1 - P_B(s)]/\nu_s\}^{1/2}.$$

The error bars reported for the experimental values of the $P_B(s)$ are calculated from the above formula. If there is no correlation at all, for a surface concentration x of the chosen adatom species,

$$P_B(s) = x$$

and

$$\sigma(s) = \sigma = [x(1-x)/\nu_s]^{1/2}.$$

In the graphs reporting the experimental $P_{\text{Si}}(s)$ or $P_{\text{Ge}}(s)$ functions (Figs. 5 and 6), there is a horizontal gray band covering the interval $x \pm \sigma$. If the Si (Ge) substitutional adatoms are randomly distributed (no correlation), then their shell occupancy probability must be shell independent and, given N adatoms, it will lie within the gray band. Thus, all the experimental points of the measured $P_{\text{Si}}(s)$ and $P_{\text{Ge}}(s)$ falling outside the band indicate significant correlations.

*Electronic address: luca.ottaviano@aquila.infn.it

- ¹A. Charrier, R. Pérez, F. Thibaudau, J.-M. Debever, J. Ortega, F. Flores, and J.-M. Themlin, *Phys. Rev. B* **64**, 115407 (2001).
- ²L. Ottaviano, G. Profeta, L. Petaccia, S. Santucci, and M. Pedio, *Surf. Sci.* **501**, L171 (2002).
- ³Y. Gauthier, R. Baudoing-Savois, J. M. Bugnard, W. Hebenstreit, M. Schmid, and P. Varga, *Surf. Sci.* **466**, 155 (2000).
- ⁴R. W. Olesinski and G. J. Abbaschian, *Bull. Alloy Phase Diagrams* **5**, 271 (1984).
- ⁵K. M. Conway, J. E. MacDonald, C. Norris, E. Vlieg, and J. F. Van der Veen, *Surf. Sci.* **215**, 555 (1989).
- ⁶M. Göthelid, M. Hammar, C. Törnevik, U. O. Karlsson, N. G. Nilsson, and S. A. Flodström, *Surf. Sci.* **271**, L357 (1992).
- ⁷A. V. Melechko, J. Braun, H. H. Weitering, and E. W. Plummer, *Phys. Rev. B* **61**, 2235 (2000).
- ⁸J. A. Kubby, Y. R. Wang, and W. J. Greene, *Phys. Rev. Lett.* **65**, 2165 (1990).
- ⁹C. Törnevik, M. Göthelid, M. Hammar, U. O. Karlsson, N. G. Nilsson, S. A. Flodström, C. Wigren, and M. Östling, *Surf. Sci.* **314**, 179 (1994).
- ¹⁰E. Ganz, F. Xiong, I.-S. Hwang, and J. Golovchenko, *Phys. Rev. B* **43**, 7316 (1991).
- ¹¹L. Seehofer, G. Falkenberg, and R. L. Johnson, *Surf. Sci.* **290**, 15 (1993).
- ¹²J. M. Carpinelli, H. H. Weitering, and E. W. Plummer, *Surf. Sci.* **401**, L457 (1998).
- ¹³L. Ottaviano, M. Crivellari, L. Lozzi, and S. Santucci, *Surf. Sci.* **445**, L41 (2000).
- ¹⁴J. M. Carpinelli, H. H. Weitering, E. W. Plummer, and R. Stumpf, *Nature (London)* **381**, 398 (1996).
- ¹⁵J. M. Carpinelli, H. H. Weitering, M. Bartkowiak, R. Stumpf, and E. W. Plummer, *Phys. Rev. Lett.* **79**, 2859 (1997).
- ¹⁶O. Custance, J. M. Gómez-Rodríguez, A. M. Baró, L. Juré, P. Mallet, and J.-Y. Veuillen, *Surf. Sci.* **482**, 1399 (2001).
- ¹⁷A. V. Melechko, M. V. Simkin, N. F. Samatova, J. Braun, and E. W. Plummer, *Phys. Rev. B* **64**, 235424 (2001).
- ¹⁸R. I. G. Uhrberg, H. M. Zhang, T. Balasubramanian, S. T. Jemander, N. Lin, and G. V. Hansson, *Phys. Rev. B* **62**, 8082 (2000).
- ¹⁹H. Morikawa, I. Matsuda, and S. Hasegawa, *Phys. Rev. B* **65**, 201308 (2002).
- ²⁰K. Binder, *The Monte Carlo Method in Condensed Matter Physics*, Topics in Applied Physics (Springer, Berlin, 1992).
- ²¹M. Polak and L. Rubinovitch, *Surf. Sci. Rep.* **38**, 127 (2000).
- ²²J. Slezák, P. Mutombo, and V. Cháb, *Phys. Rev. B* **60**, 13 328 (1999).
- ²³E. Vives and A. Planes, *Phys. Rev. B* **47**, 2557 (1993).
- ²⁴H. Stadler, W. Hofer, M. Schmid, and P. Varga, *Phys. Rev. B* **48**, 11 352 (1993).
- ²⁵A. V. Melechko, J. Braun, H. H. Weitering, and E. W. Plummer, *Phys. Rev. B* **61**, 2235 (2000).
- ²⁶B. Ressel, J. Slezák, K. C. Prince, and V. Cháb, *Phys. Rev. B* **66**, 035325 (2002).
- ²⁷J. Ortega, R. Pérez, and F. Flores, *J. Phys.: Condens. Matter* **14**, 5979 (2002).
- ²⁸G. Ballabio, S. Scandolo, and E. Tosatti, *Phys. Rev. B* **61**, R13 345 (2000).
- ²⁹D. A. Lavis and G. M. Bell, *Statistical Mechanics of Lattice Systems* (Springer, Berlin, 1999), Vol. 1.
- ³⁰C. J. Karlsson, E. Landemark, Y.-C. Chao, and R. I. G. Uhrberg, *Phys. Rev. B* **45**, 6321 (1992).
- ³¹M. Gómez-Rodríguez, J.-Y. Veuillen, and R. C. Cinti, *Surf. Sci.* **377**, 45 (1999).
- ³²B. Ressel, C. Di Teodoro, G. Profeta, K. C. Prince, V. Cháb, and L. Ottaviano (unpublished).